The Development of Ion-Etched Phase Plates

Laser-driven implosion experiments on the OMEGA laser depend on optical phase conversion to provide uniform irradiation onto a target. Phase errors that accumulate as a wavefront propagates through the laser produce a nonuniform irradiance when focused into the target far field. The distributed phase plate (DPP) introduces a quasi-random phase front that produces a high-spatial-frequency, uniform pattern with a controlled energy envelope.[1] DPP's are used in conjunction with smoothing by spectral dispersion (SSD) and distributed polarization rotation to provide very smooth intensity distribution on the target when integrated over the full pulse duration of the laser.[2]

The continuous DPP is an improvement over earlier binary designs.[3] The binary phase plates used on the 24-beam OMEGA produced a uniform irradiation with limited control over the intensity envelope and a maximum of 78% efficiency with much of the lost energy coupled into higher diffractive orders. In OMEGA's target chamber geometry this diffracted light would cause catastrophic damage in the opposing beam optics, especially the frequency-conversion cell. The more recent continuous phase design offers better control of the speckle distribution and the envelope function while increasing the total energy impinging on the target to 96%. In addition to a continuous profile, the newer DPP design requires a deeper surface relief of approximately 5 μm. The binary DPP required only a surface relief of 0.3 μm between diffractive cells.

The principle of the continuous DPP's has been demonstrated and tested using a replication process.[3,4] The required pattern is generated as an amplitude modulation in photographic film and used to expose a photoresist-coated substrate. When developed, the relief pattern in the resist is coated with a release layer and then molded in epoxy supported by another silica substrate. After curing, the epoxy is separated from the master, the remnants of the release layer are removed, and the final epoxy negative relief is coated with a water-based sol-gel antireflection coating. Unfortunately, after exposure to many high-energy laser pulses, the epoxy material developed a high absorption peak near 351 nm and after 100 laser shots began to show a high level of damage. The ion-etched DPP was developed as a remedy to the failed, replicated epoxy phase plates. Much of the technology developed for the epoxy phase plates was successfully transferred to the newer etching method. This article emphasizes the technology developed exclusively for the ion-etched phase plate and will not delve into the details of phase-plate design, methods for making a master, testing methods, or target performance results with DPP.

Key Technical Issues for Ion Etching

The problems posed in etching DPP's are unique. While ion-etching methods are commonly used in the semiconductor industry, they are typically used for binary patterns with etch depths rarely exceeding 1 μm. Diffractive optics, which do have continuous profiles, are made typically on substrates much smaller than the required 30-cm aperture of the OMEGA laser, and once again usually have smaller etch depths. Experience with large optics, familiarity with broad-beam ion sources, and a short development period led to an intensive internal development program.

The ion-etch scheme used by LLE is shown schematically in Fig. 74.1. A positive image of the photoresist master will result after etching, unlike the negative image produced with replication. This does not affect the performance of the DPP; positive and negative profiles have the same far-field performance. The positive image does have an effect on the type and number of near-field defects (discussed in detail later).

An inert ion process was used for etching the DPP's. Inert ion etching (or ion milling) depends on molecular impacts (sputtering) for materials and is a purely physical process. Reactive processes were developed for high material-removal rates in a high-production environment, production of steep edges for semiconductor interconnects, and material selectivity to preserve masks. The intensity exposure mask for continuous DPP design in Fig. 74.2 has low gradient (no steep edges), and material selectivity is not as important as faithful reproduction of the photoresist surface. This last requirement demands that the etch depth be linear with time for both materials, which

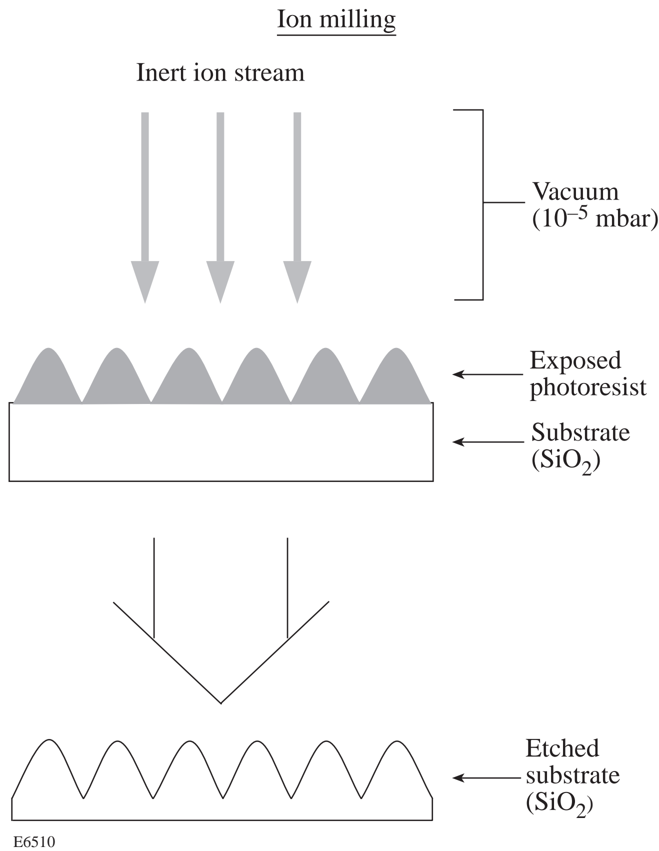

Figure 74.1
A surface-relief phase plate can be directly etched from a photoresist pattern into a silica substrate. The photoresist is completely removed after etching is complete. The etching molecule in this work is an inert gas, argon, so removing the photoresist and silica is purely a physical process.

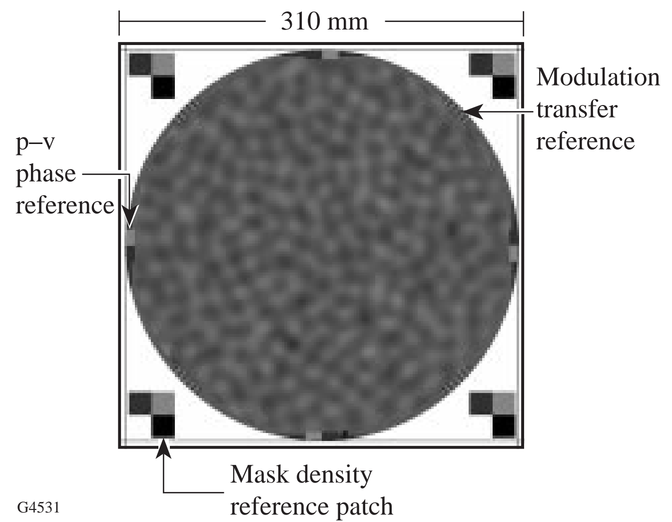

Figure 74.2
The continuous DPP for the third-order super-Gaussian profile used on OMEGA was designed using simulated annealing. The amplitude variation of the mask is transferred into phase variation by exposing the photoresist to the mask. The central portion of the mask was modified after design to provide a high point in the resist for in-process optical monitoring.

is more likely in a purely physical process. Complete erosion of the mask is necessary since any remnant photoresist could be the potential site for laser damage in the 351-nm radiation. Since LLE has had little previous experience with reactive processes, inert ion etching was the method of choice.

A number of key technical issues had to be resolved before DPP's could be produced:

1. Uniformity

The uniformity of etch across the 280-nm beam aperture had to vary less than 6% after 5 μm of material was removed. This was accomplished by first using two 8-cm ion sources with the substrate in single rotation and, later in the project, a single 16-cm ion source, also with single rotation. After establishing the correct operating parameters for the guns, all were profiled at different beam voltages and total ion currents using a biased ion probe. The profiles were used to calibrate a model of etch uniformity that was developed to determine the best source location and pointing for high uniformity and reasonable etch rate. It is well known that the sputtering yield varies considerably with the ion incidence angle in inert ion etching.[5] The relationship between etch rate and incidence angle had to be determined for the two etch materials: silica and photoresist.

2. Surface Texturing

Surfaces are often textured after a high level of ion bombardment.[6,7] Silica surfaces have been observed to become rougher or smoother depending on the type of ion, ion energy, incidence angle, and ion density.[8,9] Texturing occurs predominantly in crystalline materials and is most often caused by the varying sputter rate of different crystal planes. Resputtering and defects in the surface preparation of a substrate have also caused texturing.[10] During development of etched DPP's, severe roughing of the surface was often observed but it was primarily caused by the overlying photoresist. Although surface texturing by ions was often suspected, the true cause appears to be excessive heating of the resist in almost all cases.

3. Linearity

An accurate representation of the photoresist master in silica can only be realized if the process remains linear throughout the etch. Proper processing of the resist and careful control of the substrate thermal cycle produced adequate linearity.

4. Near-Field Defects

Near-field defects are caused by small and steep surface variations in the photoresist layer, which cause diffraction and high intensities downstream of the DPP. These defects have a strong potential to damage the final focus lens and blastshields on the target chamber. Near-field defects were first observed in the fabrication of the first set of continuous epoxy DPP's for OMEGA. Methods for detecting and removing the defects were established for the epoxy DPP's and then modified for the ion-etched devices.

5. Production Tooling

Resputtering of tooling materials will cause higher absorption and scatter on the ion-etched surface. In addition the tooling must allow a clear view of the rear surface to radiate heat to the cooled cryopanels. The tooling design offered a unique solution to these requirements.

6. Laser-Damage Threshold

When measured at 351 nm, some ion-etched samples have shown a decrease in damage threshold. This could be caused by resputtering of ion sources, tooling, or chamber materials onto the optics. The damage threshold of the DPP's had to meet a 2.6 J/cm^2 @ 1-ns peak fluence requirement for the 351-nm OMEGA beam. The damage threshold of the DPP surfaces increased after etching, probably due to careful control of redeposition of tooling and removal of subsurface damage in the silica.

Each of the technical issues listed above is discussed in detail below.

Uniformity of Ion Etching with a Kaufman Source

The Kaufman[11] ion source, originally developed as a propulsion source for NASA, has since seen wide use in materials processing.[12] The source, shown schematically in Fig. 74.3, consists of a discharge chamber with a multipole magnetic field and a hot filament, two dished molybdenum extraction grids, and a neutralizer filament. Two 8-cm ion sources were used for prototype demonstration, and a 16-cm ion source was used for the production phase of this work.

Ion-source parameters are set depending upon the application, type of working gas, and performance of the source in a given pumping system. Argon was used as a working gas because the sputter yields for SiO_2 and photoresist are similar for this gas. The maximum gas flow rate, maximum beam current, and accelerator voltage range for the sources were determined using standard methods.[13] The beam voltage (ion energy) was kept below 500 V to avoid ion implantation, surface damage to the photoresist, and overheating.

The etch profiles of each source were tested using a unique profiling method: A large sheet of inexpensive float glass was coated with an optical multilayer that had a highly visible, 13-layer oxide coating (see Fig. 74.4). The coated plate was placed normal to the ion beam at a distance of 60 cm. The source was run long enough to etch to the last layers of the coating; the coating was then removed and inspected. The erosion pattern could then be discerned as contours in the multilayer surface (see Fig. 74.5). This method gave a very quick appraisal of the gun operation and indicated whether the profile would be suitable for highly uniform etching. For

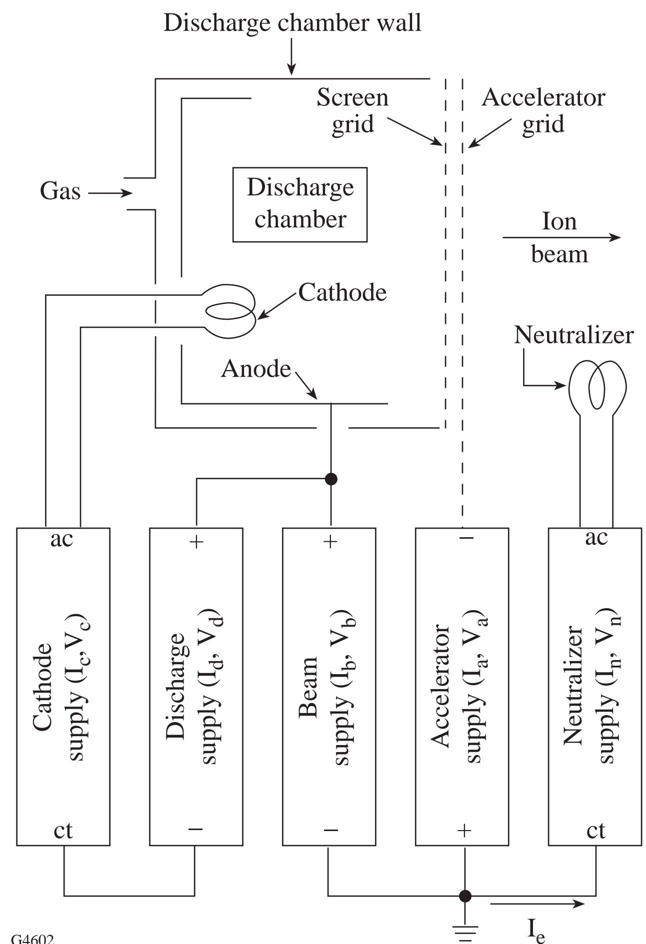

Figure 74.3
A typical broad-beam Kaufman ion source with power supplies is represented schematically. This type of source provides excellent control of ion energy and density. The source's condition during etching can be monitored by logging the voltage and current of each supply.

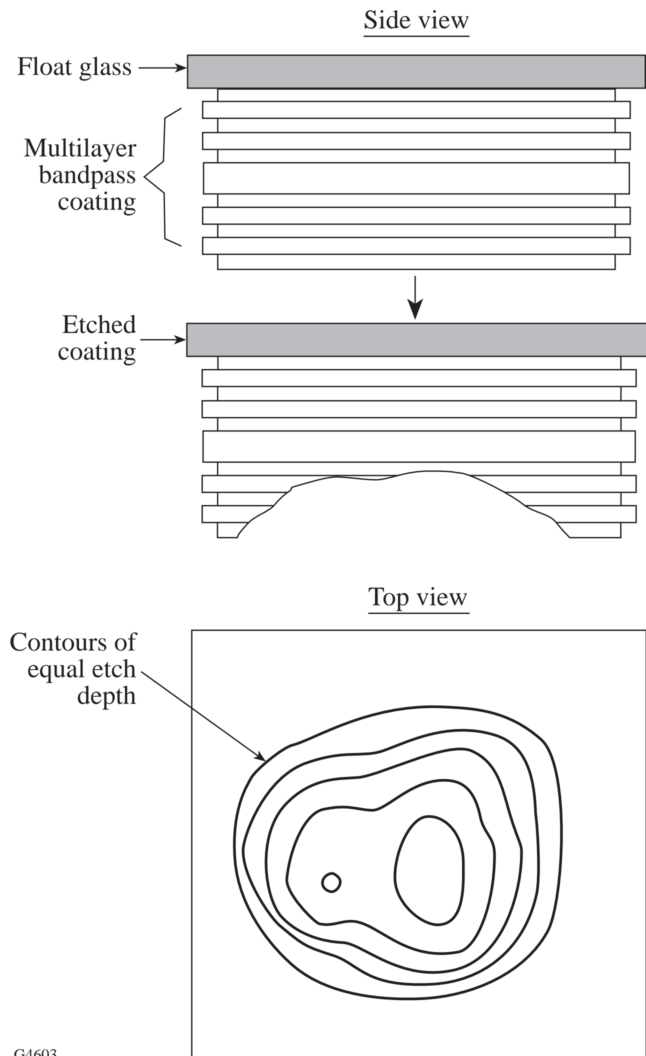

Figure 74.4
Ion-beam profiles can be monitored with a small probe or by etching into a visible interference filter deposited on inexpensive float glass as shown. The beam contours are formed by the eroded layer of the coating. After etching, the layers in an appropriately designed multilayer provide visible isothickness contours, indicating the beam profile of the ion source.

example, the etched profile of the 8-cm source operating at a beam current of 100 mA is shown in Fig. 74.5(a). Even though the source was within the normal electrical limits (low ion impingement of the grids), the profile has significant structure. The same source produced a low-structure symmetrical profile when operated at 50 mA [Fig. 74.5(b)] and was subsequently used with beam currents (I_b) no larger than 75 mA. The condition of the source anode also had a significant effect on the beam profile. The anode can be run in excess of 60 h before a discharge becomes difficult to maintain, as seen in Fig. 74.5(c); however, the beam profile again shows structure with the older anode. If the anode is abrasively cleaned, the structure in the beam profile disappears. The 16-cm source was later characterized in the same manner. Figure 74.5(d) shows the symmetrical beam profile of the source when operated with I_b = 300 mA and a beam voltage of 150 V.

The gun profiles were quantitatively measured with an open stainless steel probe after the initial gun characterization to determine the operational limits of the sources. For these measurements the ion probe was negatively biased with 18 V to repel the low-energy electrons in the beam. Both the 8-cm and the 16-cm sources were characterized at heights from the source grids ranging from 20 cm to 85 cm. The 8-cm source profiles were observed under varying conditions to determine which parameters affected the beam profile. Certain parameters, such as low neutralization current and high chamber pressure, had little effect on the profile. The most significant effect was a buildup of an insulating film on the anode, as noted above with the multilayer etch profiles. Significant differences seen in profiles between the two 8-cm sources were attributed to differences in the magnetic field surrounding the discharge chamber.

The 16-cm source beam profile is exceptionally immune to changes in the operating parameters. Profiles taken under a range of operating conditions and normalized at the on-axis center (r = 0) are compared in Fig. 74.6 for a fixed height above the source. In practice, the similarity in profiles allows use of the source over a wide range of ion energies and densities without making large changes in the geometry established to produce uniform etching. A single model, independent of source parameters, was used in the uniformity code discussed below.

Etching Model

Processes that use energetic ions for large substrates require that the time-averaged erosion effects from the ion flux be uniform across the surface. A numerical model has been developed to determine this flux and its effects on surface etching of a silica/photoresist combination. The geometries of the source and substrate are very similar to typical deposition geometries with single or planetary substrate rotation. The model was used to tune an inert ion-etching process that used single or multiple Kaufman sources[14] to less than ±3% uniformity over a 30-cm aperture after etching 5 μm of material. The same model can be used to predict uniformity for ion-assisted deposition (IAD).

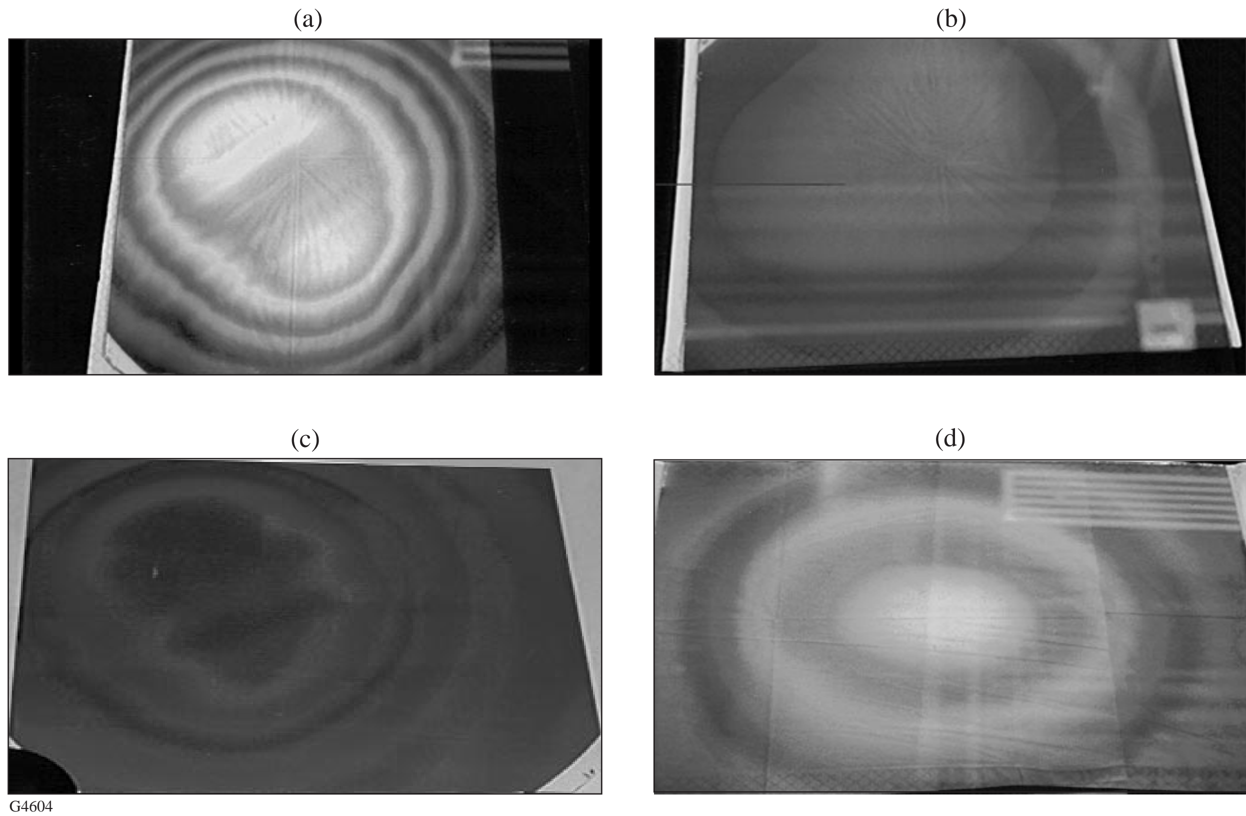

Figure 74.5
The beam profiles formed in the etched multilayers provide rapid feedback to determine correct operating limits and procedure with the ion sources. (a) Profile of a nonuniform etch obtained with the 8-cm source at an excessive beam current (I_b = 100 mA). The structure is a partial image of the spiral filament for the discharge chamber. (b) A profile from the same source as in (a) at lower beam current (I_b = 50 mA). (c) The 8-cm source operated at low current but with a contaminated anode, which had been used previously for 30 h without cleaning. The thin dielectric film that forms on the anode has an obvious effect on the discharge and beam uniformity. (d) The 16-cm source etched uniformly even when used at beam currents as high as 300 mA.

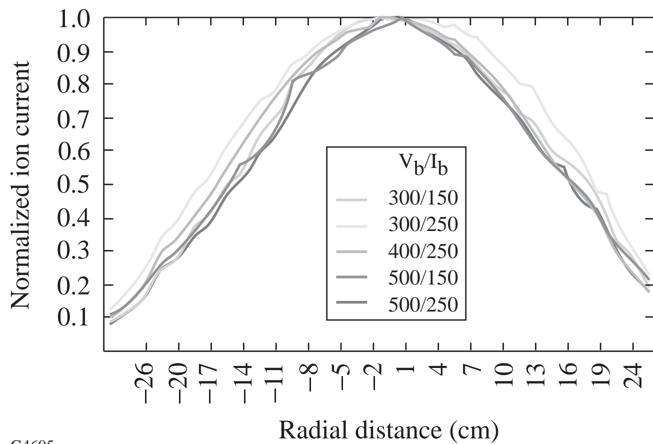

Figure 74.6
The 16-cm source had a stable profile over a wide operating range. The first number in the key is the beam voltage, and the second number is the beam current (in mA). All curves are normalized at $r = 0$.

In Fig. 74.7 an ion source is placed in some arbitrary location and orientation with a substrate rotating in a horizontal plane above the source. The total ion beam flux seen by a point P on a substrate at some radius r from the center can be approximated by

$$E(r) = \sum_{\phi=0}^{\phi_{\max}} I(\phi, r) R(\phi, r) \Delta\phi, \quad (1)$$

where $I(\phi, r)$ is the ion flux intensity determined at point ϕ, r and $R(\phi, r)$ is the sputter yield at the same point. R is actually a function of a single variable, the incidence angle of the ion,[15] but both ϕ and r are required to determine this angle. In reality, point P will see a range of incidence angles due to the broad nature of the source. Here, a point source is assumed using the top center of the ion-source grid as the origin of ions, and a single incidence angle is used for the approximation. The example in the diagram shows a simple single rotation of the substrate. For this case, $\phi_{\max} = 2\pi$ represents one full rotation of the substrate and is adequate to model the uniformity. A more complex double rotation (planetary) can also be modeled. In that case the point P traces out an epicycloid instead of a circle.

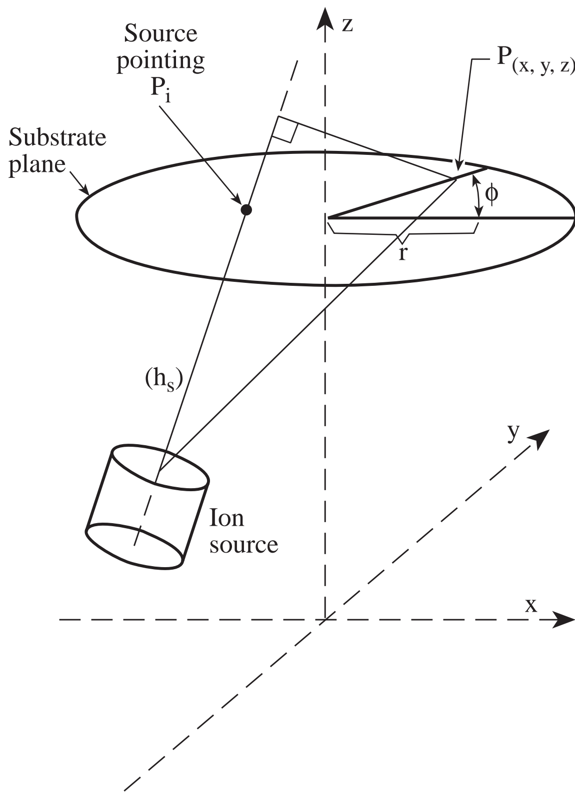

Figure 74.7
Geometry for ion etching with substrate rotation in the horizontal plane. To adjust the uniformity the source pointing was fixed, and then the source was moved on a rail along the x axis.

The model described by Eq. (1) can be broken down into three major parts:

1. summation and location routine: simulates the position of a point on a substrate, finds all position and angular parameters, and integrates the calculated flux through some amount of substrate rotation;

2. expression for $I(\phi, r)$: a model for the expected ion flux that is determined from measured values of the ion source; and

3. expression for $R(\phi, r)$: a relationship between the incident ion angle and energy and the sputtering yield (or etch rate) of the substrate. This also must be determined experimentally.

The model for $I(\phi, r)$ assumes a rotational symmetry of ion density about the axis normal to the ion-source grids.[16] This is a reasonable assumption if the discharge chamber in a hot-cathode source is maintained and cleaned regularly as discussed previously. At a given height h_s above the source, the data can then be fitted to a 1-D super-Gaussian equation

$$I = a + be^{\left(-\left|\frac{r-c}{d}\right|\right)^{e}}, \quad (2)$$

where I = ion flux/area for a given r, a = dc offset (usually set to zero), b = amplitude factor at $r = 0$, c = offset for r (set to zero for well-centered beams), d = width factor, and e = shape factor.

The factors b, d, and e all vary with the height above the source. In practice, the beam profile is measured at various heights, and each profile is fitted to Eq. (2). The values found for b, d, and e at various heights are then fitted to curves using a commercial curve-fitting program. The resulting equations and associated coefficients can then be written into a concise code for modeling. Some results of the measured values and the model are given in Figs. 74.8(a) and 74.8(b). The model provides a smoother profile than the actual measured data. This is reasonably accurate since smoothing would also occur in the actual source data if the profile was an average of measurements at some fixed radial distance around the source.

The expression for $R(\phi, r)$, the etch rate as a function of ion incidence angle, was also determined experimentally. Small silica plates with binary photoresist patterns were mounted on miniature rotation drives with the axes set at 20°, 30°, 40°, 50°, 60°, and 0° to the beam axis (see Fig. 74.9). The center of each substrate was placed on a circle, and the entire assembly was rotated in the horizontal plane during the etch; thus, with the ion source on axis, the ion-etch rate for silica and photoresist could be determined simultaneously for six incidence angles by measuring step heights and photoresist thickness. Data were obtained for different operating source parameters and

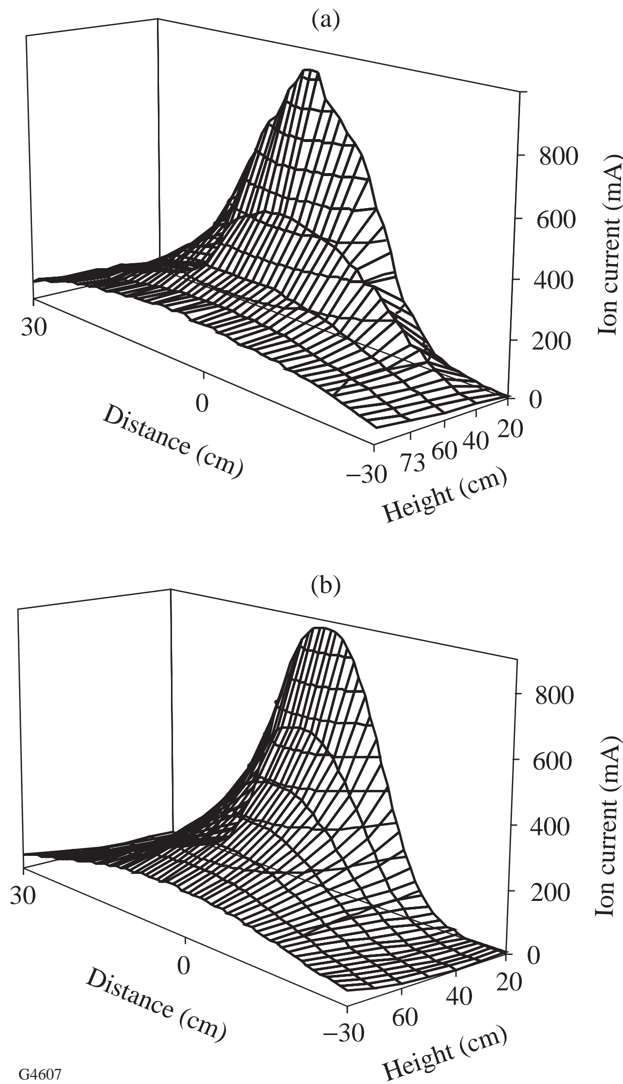

Figure 74.8
(a) Measured profile of the 16-cm ion source operating at 300-V beam voltage and 250-mA beam current at different heights above the grids. (b) Model of measured profile in (a). This model was used in the uniformity program to determine placement of the ion sources.

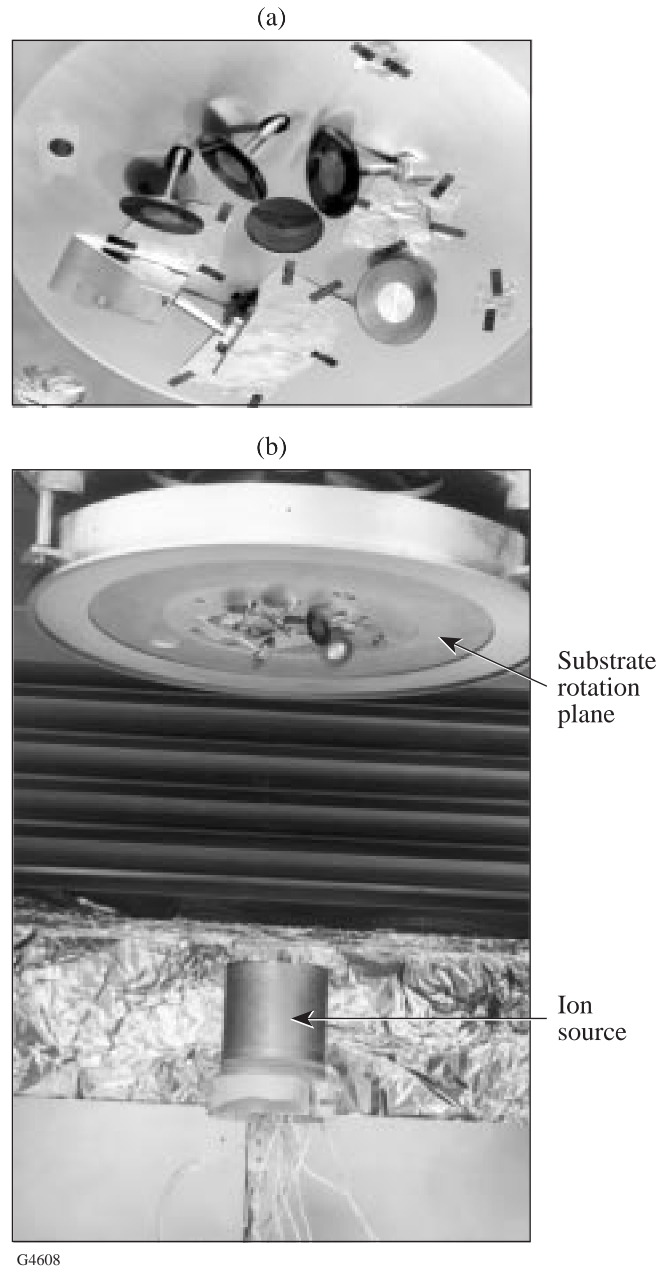

Figure 74.9
(a) The apparatus to measure the etch rate for silica and photoresist simultaneously for several ion incidence angles. Each substrate has a binary pattern of photoresist and is attached to the shaft of a motor. (b) The ion source was placed directly below the apparatus while the entire substrate apparatus above was rotated to obtain a uniform average ion flux density on all test pieces. Substrate heating affected the consistency of results in this experiment.

photoresist preparation processes. The data were often obscured by measurement errors and problems with surface roughening. The original intent was to generate curves for different photoresist annealing conditions (see Fig. 74.10) and to pick the curve that most closely matched the silica curve. In practice, the measurement was flawed by the inability to cool the samples during etching, which increased the apparent etch rate on photoresist. Thus, from these results, the etch rate of photoresist appeared higher than that of silica, but later, on cooled substrates, the etch rate of resist proved to be lower than that of silica.

Since the two materials did etch at different rates but appeared to follow the same curve, the curve for the photoresist annealed at 110°C was selected for the model. The normalized data from this measurement experiment were fitted to a polynomial of the form $y = l + m\theta^2 + n\theta^{2.5} + o\theta^3$. The data and the fitted curve are shown in Fig. 74.11. The accuracy of this data (due to thermal effects) is the largest source of error for the model.

The results for the full uniformity model using the 16-cm source demonstrated that the source should be able to etch a 30-cm aperture uniformly without requiring a supplemental 8-cm source for fine adjustments. Typical results from the full model are shown in Fig. 74.12. The array of curves demonstrates what effect moving the source on a path parallel to the

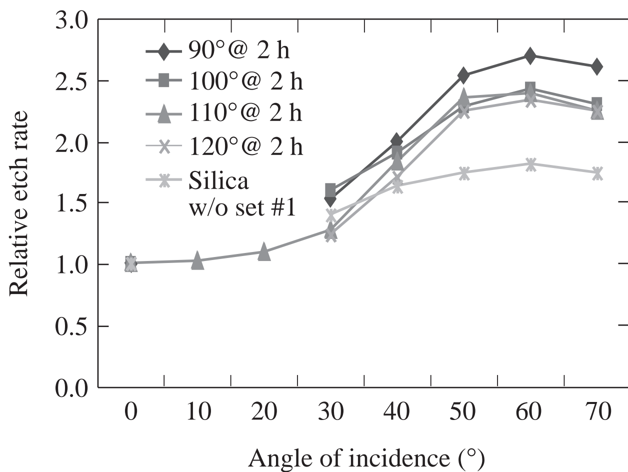

Figure 74.10
The measured etch rate versus ion incidence angle for photoresist anneal after development at different temperatures. Substrate heating affected the consistency of results for photoresist in this experiment. The silica measurements, which are more consistent, are included for comparison. All etch rates have been normalized at 0° for comparison.

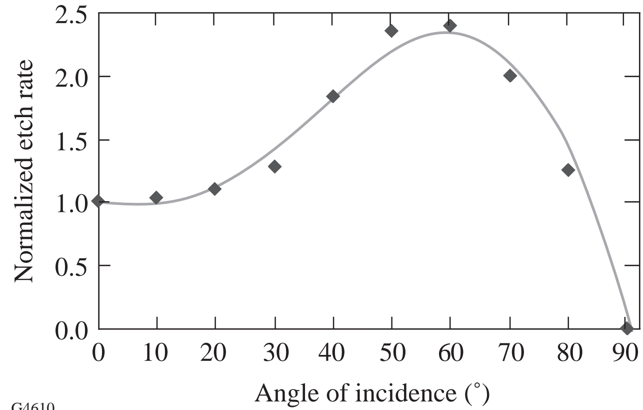

Figure 74.11
The photoresist data for resist baked at 110°C were fitted to the equation $r = \ell + m\theta^2 + n\theta^{2.5} + o\theta^3$ for the uniformity model. Some data were assumed based on other results investigating angular dependence of sputtering.[15] A zero rate was assumed for 90° and values were estimated for 10° and 20°, which satisfies the condition for an increasing positive first derivative.

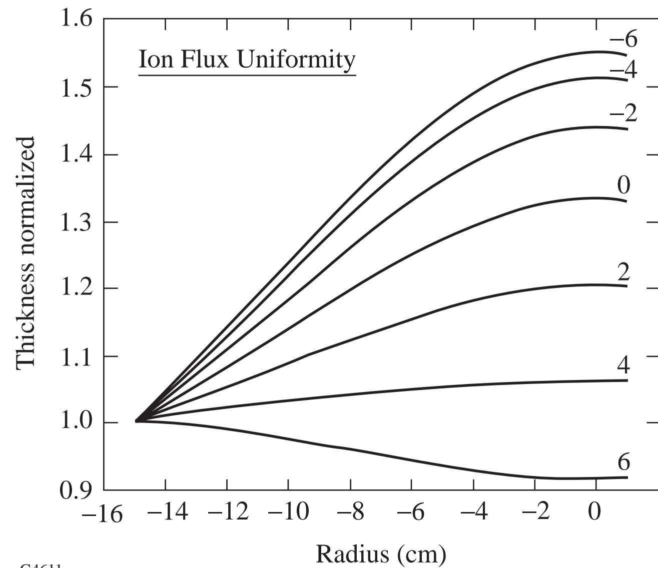

Figure 74.12
The uniformity model is used to evaluate gun positions for one or several ion sources. The graph shows the thickness of material removed, normalized to the first value at −15 cm, as a function of the radius along a DPP-sized substrate. The axis of the source struck the substrate plane at a 30° angle, and the ion-source grid center was placed 34 cm below the substrate. The source was pointed −11.5 cm from the x axis, and the curves represent the change in uniformity as the source is moved along the x axis (*x*-pointing value in centimeters is shown with the curve). This model was reflected in the hardware arrangement with the source on a rail that could easily duplicate the movement along the x axis. The model revealed that a uniform solution could be achieved with the single 16-cm ion source and indicated the sensitivity of positioning. The final position of the source was finally adjusted empirically for best uniformity.

x axis and away from the substrate has on uniformity. The ion-source axis is at 30° with respect to the substrate's normal axis, and the source is pointed away from the center. The model also tracks total integrated current for the starting point, which is used to determine the efficiency of a given geometry. Figure 74.12 shows that a uniformity of better than 7% could be achieved with careful pointing of the source. In practice, etch uniformity of less than 2.5% was measured and, during production of 60 optics, was kept below 6% across the 30-cm clear aperture.

The model was also used early in development to optimize the uniformity of two 8-cm sources etching simultaneously. The model did not always fit the exact results from the chamber; however, it did offer guidance in selecting which direction to move a source while final tuning was completed empirically. The best uniformity results were obtained with the source pointing outside the clear aperture. In this case, most of the ions did not strike the substrate, and the process made inefficient use of the generated ions. A double-source arrangement with a 16-cm and an 8-cm source could have greatly decreased the total etch time but only at the expense of decreased reliability and possible overheating of the photoresist. The 14-h etch time required for the approximately 5-μm etch into fused silica meshed well with the production rate for exposed photoresist-coated plates.

Uniformity Testing

The most reliable test of etch uniformity is to etch directly in silica or photoresist and measure the change in surface profile using interferometry. This method requires a surface that is flat enough to accurately test both before and after the etch. A uniform photoresist coating was applied to a flat-polished substrate, then was partially etched and measured. The substrate could then be stripped of the photoresist and reused without repolishing. The surface measurement prior to etching was stored and subtracted from the post-etch measurement to provide the true etch profile. One sample, if coated with 7 μm of photoresist, could be used several times for uniformity tests during development and as a quality check during production. A sample result of interferometry after etching a photoresist surface is seen in Fig. 74.13. The flat is measured in transmission by placing it in a Fizeau cavity and observing the change in wavefront. The height variation in the resist surface layer is then found from

$$d = \frac{\text{OPD}}{(n-1)} \bullet \frac{\lambda}{2}, \tag{3}$$

where OPD is the optical path difference in waves and n is the refractive index of the photoresist at the test wavelength λ. The factor of 2 compensates for the round-trip path the wavefront travels when transmitting through the optic in the cavity.

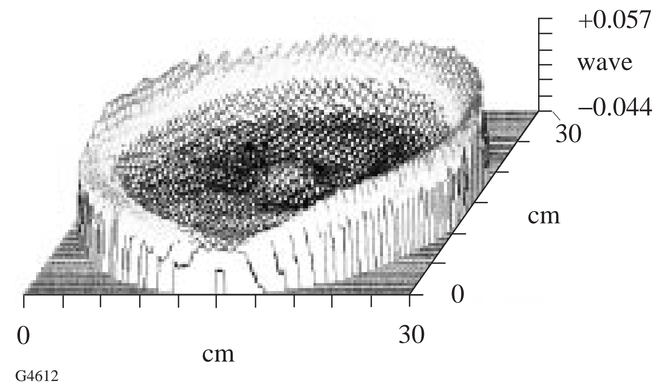

Figure 74.13
The surface figure of an etched photoresist coating measured in a phase-shifting interferometer. The surface figure prior to etching is subtracted from this measurement. The peak-to-valley and rms height values are 0.107 and 0.011 waves, respectively, measured at 633 nm. The overall power is removed from the data. Data from these measurements are combined with the total etch depth measured in the center to determine the etch uniformity in the following figures.

The plate is also tested at the center of the etched surface with a spectrometer to determine the total thickness of the photoresist coating before and after the etch. The total etch depth is found for the center and is combined with the interferometric data to generate a profile of the material removed by etching. This profile is divided by the average thickness of the etched material to provide a normalized etch uniformity for run-to-run comparison. Several profiles from the development and production phases are seen in Fig. 74.14. Figure 74.14(a) shows the convergence toward a good uniformity during the development phase. At the end of tuning the uniformity had a variation of less than 4%. Figure 74.14(b) shows the short-term stability (run-to-run) of uniformity attained during the final calibration sequence prior to etching the phase plates. The plots in Fig. 74.14(c) demonstrate the long-term stability of the etch uniformity over the 6-month production sequence of the phase plates. Stability was maintained by accurate positioning and pointing of the ion source and careful monitoring of the discharge electrical characteristics during source operation. Plots from the model in Fig. 74.12 suggest that maintaining pointing and position of the source to within a few millimeters should be adequate to limit variation in the uniformity to ±1%.

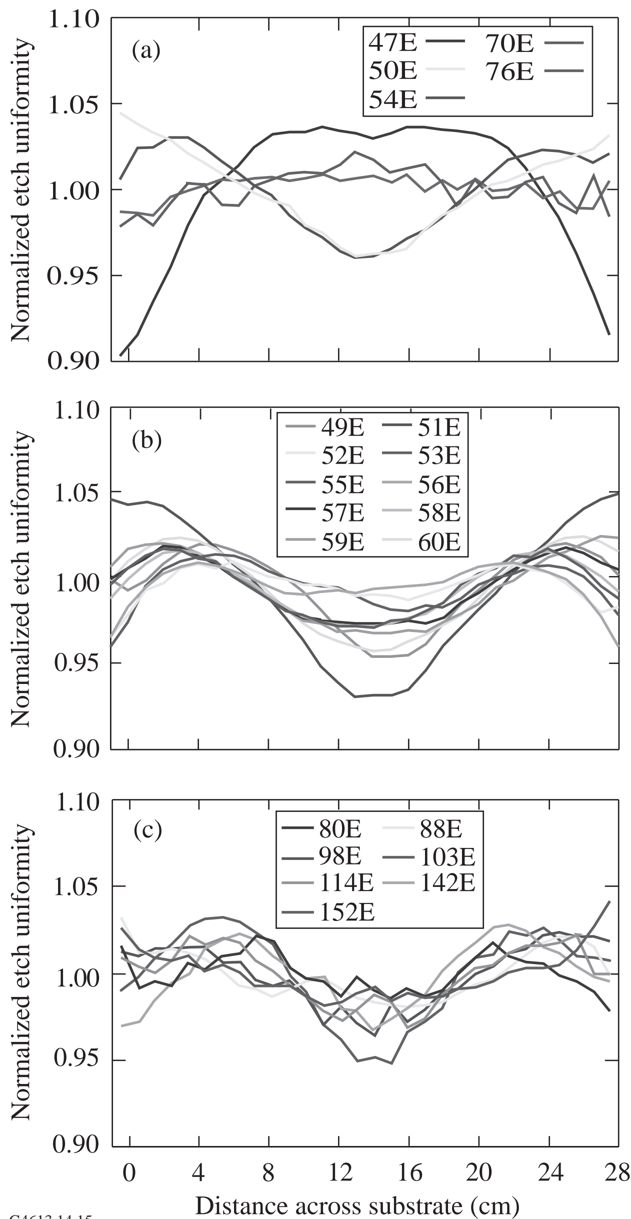

Figure 74.14
Plots of the normalized etch uniformity over the optic clear aperture during different phases of the project. (a) Good uniformity was achieved fairly quickly during the development stage as the ion source was adjusted to its final geometry. (b) The uniformity of sequential etch runs prior to production (calibration sequence) demonstrated the high repeatability of the process. The one run that deviated from ±2% was etched with a slightly different geometry. (c) The etch uniformity was very stable over the 8-month production period. The uniformity was periodically checked by etching flat, unexposed plates of photoresist. Gun position was checked frequently during production to maintain this uniformity. The numbers labeling the curves correspond to the sequential etch run for a given year.

Texturing Problems

Increasing surface roughness and scatter potentially limit the usefulness of ion-etch methods in optical applications. Surface texturing is well documented in ion-beam applications and has been attributed to several erosion-induced morphological changes including

a. development of cones and pyramids due to the angular dependence of the sputter yield;

b. faceting of different crystal planes in a polycrystalline material; and

c. redeposition of contaminating materials onto the mask and substrate. This causes local regions of different sputter yield that evolve into a structure surface.

The incidence angle tests were designed in part to test the effects of texturing from cause (a) listed above for silica and photoresist. Faceting (b) should not occur in either material since both are amorphous. Redeposition of metals, especially from tooling, was a concern and is addressed later. Other texturing effects in silica have been studied[9] but are generally found to occur at high incidence angles and at ion energies an order of magnitude higher than those used in this study.

The first experiments to probe the angle dependence on sputter yield tended to develop scatter on samples held normal to the ion beam and less so on the samples oriented at 60°, 50°, 40°, and 30° with respect to the incoming ion beam. The broad range of morphologies of the scatter in photoresist are seen in Fig. 74.15. The scanning electron micrographs (SEM) showed blistering in one view [Fig. 74.15(a)], while the other view [Fig. 74.15(b)] gave the impression of melting and flowing resist. Atomic force microscopy (AFM)[17] revealed high spatial frequencies in some areas of the photoresist scatter in Fig. 74.16(a). Areas where the photoresist had been fully eroded showed a different morphology [Fig. 74.16(b)]. The high spatial frequency component was absent here, and the surface was dominated by smooth, shallow depressions. The change of morphology of the silica surface is probably due to some planarization associated with the angular dependence of ions. This morphology occurred only in silica that was underneath the textured photoresist. Areas covered by only a very thin layer of resist showed no scatter related to etching. This evidence led to the conclusion that the photoresist was heating up, nearing its softening point, and beginning to flow during the etch.

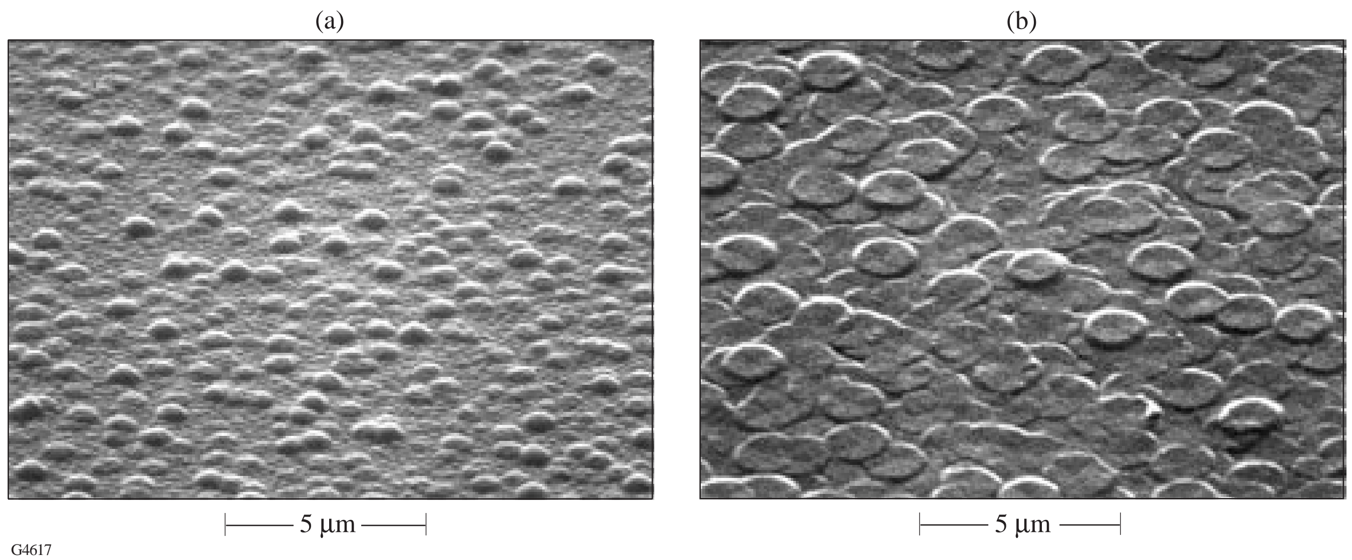

Figure 74.15
Scanning electron micrographs showing the different morphologies of high-scatter photoresist areas after etching. (a) and (b) are samples from ion-etch experiments to determine angular dependence of sputter (Fig. 74.9). The surface in (b) shows distinct signs of flow as the photoresist temperature rose during etching.

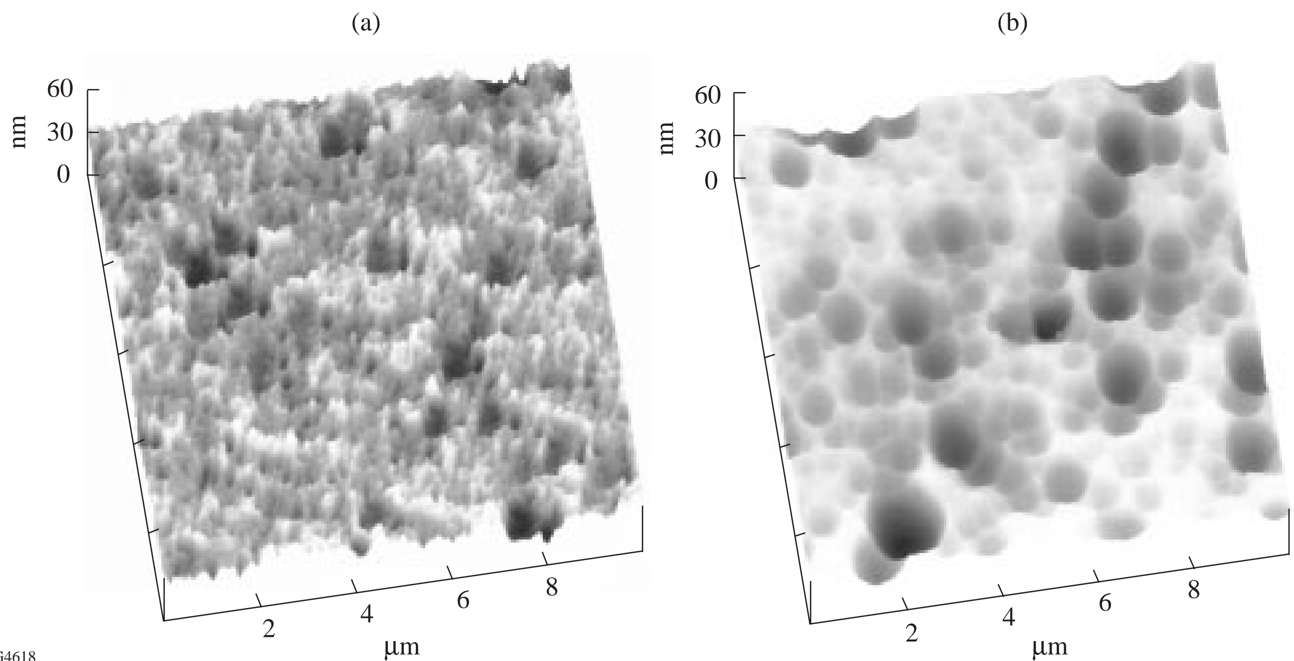

Figure 74.16
AFM scans of the surface of a 30-cm, partially etched substrate. High-scatter areas where photoresist remained (a) were measured as well as areas where photoresist was completely eroded away and only silica remained (b). The roughness in the resist area (a) seeded the topology of the SiO_2 surface (b). The morphology in the silica was then modified further by classical sputtering effects of angular dependence of sputtering, ion reflection, and redeposition.

The primary radiative thermal load during ion etching is the hot ion source and associated filaments. A secondary thermal load comes from the ion impingement, which provides an average energy of 0.1 W/cm^2 directly onto the surface of the resist; however, much of that energy is transferred by momentum to the etched molecule. In the angular dependence experiment the heat load would be largest for the substrate that had the largest amount of surface area exposed to the heat source, e.g., the normal incidence sample that typically had the highest scatter. To test this hypothesis a thermal sensor was placed directly above a rotating DPP master (a substrate with a full-thickness photoresist coating) to sense the temperature of the back of the substrate during etching. The temperature was monitored while the ion source was operated intermittently to allow the substrate to cool after a period of etching [Fig. 74.17(a)]. When the substrate was prevented from going above 50°C, the photoresist did not develop a textured surface. The surface of the photoresist layer must be significantly hotter

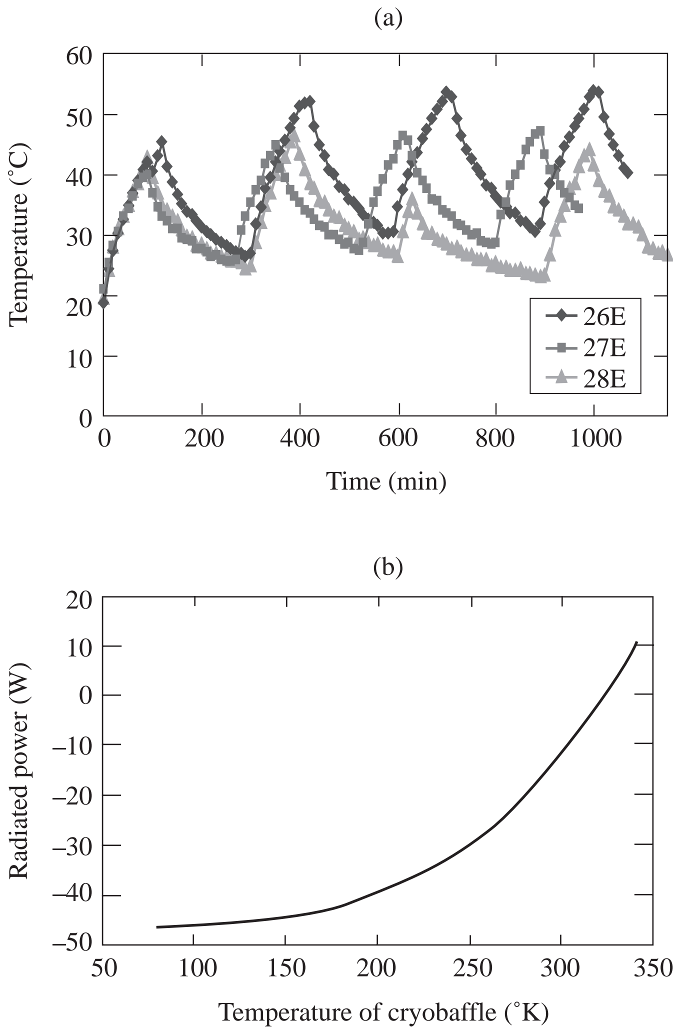

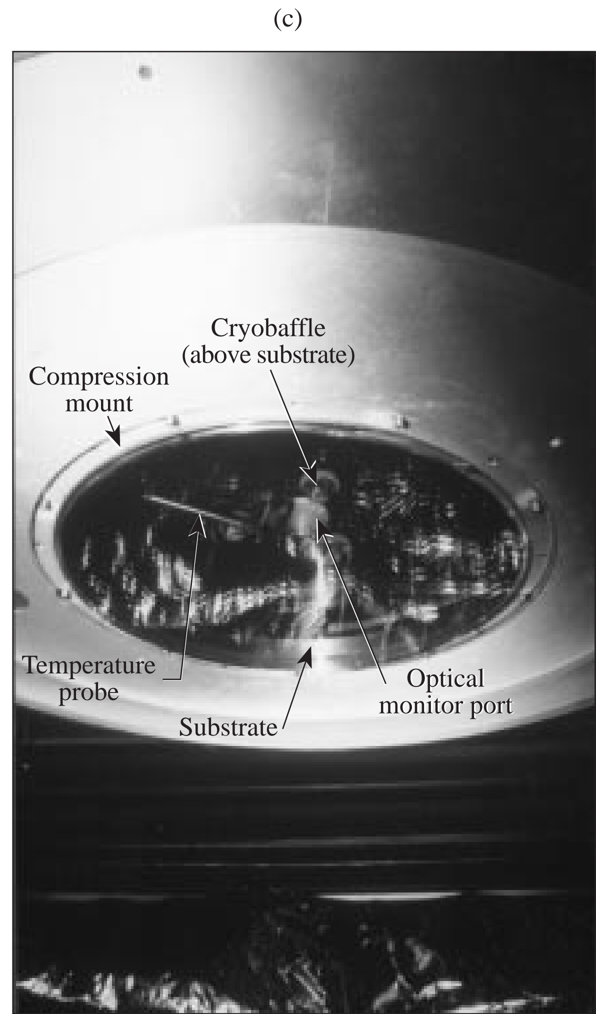

Figure 74.17
(a) The ion sources were operated intermittently in this test to allow the substrate to cool between etch cycles. The temperature of a probe close to the substrate is plotted versus time for several intermittent etch runs. Surface scatter in the resist became prominent when the measured probe temperature exceeded 50°C. A thermal load of 15 W (from the ion source) was calculated from the rate of temperature rise of the substrate. (b) The radiative heat transfer power of the cryobaffle on the back of the substrate has the capacity to cool the substrate if the baffle is cooled at liquid nitrogen temperatures. The calculation assumes the DPP is at 323°K and the emissivity of both the cryobaffle and the substrate are unity. (c) The DPP substrate is seen in the compression chuck. The cryobaffle is above the substrate with a temperature probe near the optical monitor port. The optic is held so it is the closest object to the ion source to prevent resputtering and redeposition from any metal hardware onto the optic surface.

than this measured temperature since softening temperatures for most resists exceed 120°C. This could not be confirmed because the front surface temperature of the rotating substrate could not be measured easily without disturbing other concurrent experiments. This test confirmed the suspicion that the texturing effect was due entirely to overheating of the resist during etching.

The immediate solution to the heating problem was to cryogenically cool the substrate from the back (top) surface. A 15-W heat load on the substrate was determined from the rate of temperature rise in the intermittent etch tests. The heat load could be reduced only by moving the ion source away from the substrate, which would result in excessively long etch runs. The thermal radiative power for two flat surfaces was found from the relationship

$$Q(T) = \sigma * \frac{T^4 - S^4}{\left[\left(\frac{1}{\varepsilon_1} + \frac{1}{\varepsilon_2}\right) - 1\right]} * A, \quad (4)$$

where $\sigma = 5.6697 \times 10^{-8}$ W°K/m^2, T is the temperature of the cryobaffle, S is the maximum allowable temperature of the substrate (323°K), A is the substrate area, and ε_1 and ε_2 are the emissivity of the substrate and the cryobaffle. Both emissivity values were assumed to be unity since the peak wavelength of radiation will be in the 5- to 10-μm range. The cooling power of the cryobaffle as a function of the baffle temperature is given in Fig. 74.17(b). A cryobaffle was designed and fabricated[18] that had temperature regulation provided by a proportioning valve for liquid nitrogen and internal heaters [see Fig 74.17(c)]. The cryobaffle could be rapidly heated after the etch completion to prevent condensation on the substrate and excessive cooling of photoresist in partially etched plates. Temperatures of probes near the front surface and between the back surface and the cryobaffle were recorded for all etch runs.

The design of the substrate mount was driven by the need to thermally cool the optic from above, to hold the optic through a wide temperature range in case of ion-source failure, and to prevent redeposition onto the back of the substrate from scattered ions. In addition, resputtering of hardware onto the front surface of the substrate was to be avoided since it would both increase localized scatter and lower the damage threshold of the optic. The mount functioned as a compression chuck and used a polyetherimide[19] material to hold the optic [see Fig. 74.18(a)]. The optic surface was located well below all other hardware, which prevented resputtering of hardware material onto the surface. A conductive metal apron dropped down around the mount from the cryobaffle above to improve cooling of the mount.

The compression mount was tightened enough to prevent the optic from releasing during a worst-case condition where, if the cryobaffle failed, the optic and mount would heat to 80°C. The stresses of the mount on the optic were modeled using finite element analysis [Fig 74.18(b)] to ensure that the optic would not fracture when placed in the cold extreme of –80°C. The compressive stresses did not exceed 400 kg/cm^2, and the tensile stresses were less than 80 kg/cm^2 [SiO_2 strength is 11,000 kg/cm^2 (compressive) and 500 kg/cm^2 (tensile)].[20] The mount with an optic can be seen in Fig.74.18(c).

The surface scatter was visibly reduced in all etch runs that were cryocooled. The only exception occurred on some DPP's that were rotated too slowly during the etch cycle and others that did not cool well enough directly under the optical monitor port in the cryobaffle. (This caused local hot spots in the optic and very light scatter.) The total scatter from any plate never exceeded a loss of more than 1% at 351 nm. AFM scans of a typical and a worst-case surface are illustrated in Fig. 74.19. The typical low-scatter silica surface after removal of 5 μm of material had an rms roughness of 3.7 nm with peaks of 24 nm, and the worst-case area had an rms roughness of 4.14 nm with peaks of 60.8 nm. The isolated peaks in the worst case are assumed to be seeded by blisters in the photoresist.

Linearity

In a continuous profile optic, a linear removal rate between the photoresist and the silica is essential. If the process were not linear, it would be necessary to modify the original mask to compensate for the nonlinearity, and to tightly control the nonlinear process from run to run. Linearity was tested by using a calibration mask designed by LLE's Optical Imaging and Sciences Group [Fig. 74.20(a)]. This mask produces a linear ramp in resist, a stepped ramp, and several steps in different locations in the aperture. It also has a flat region across the center that can be used to measure etch uniformity. The ramp region, which was the most useful, was measured on an interferometer[21] before and after etching. A typical result from the measurement is seen in Fig. 74.20(b).

The ion-etch pattern faithfully reproduced the ramp in the photoresist master. The normalized measured ramps of the photoresist ramp and the etched silica ramp from this master are compared in Fig 74.20(c). The departure from the photore-

sist curve for the thicker resist is due to some residual spatial nonuniformity that existed in the process at the time of the test. The ratio of the slopes of the silica ramp to the photoresist ramp was approximately 1.3 during a calibration sequence just before production. This value represents the etch ratio of the two materials and depends on the photoresist type, resist bake parameters, ion incidence angle, and ion energy. The higher etch rate in the silica allowed for the use of lower thickness photoresist coatings and reduced exposure times to the mask for a given desired spot size of the DPP. The final resist thickness for this design was 3.5 μm, which produced a 5-μm peak-to-valley pattern in the silica. The ramp of the silica is plotted against the straight line target in Fig 74.20(d). The linearity seen in this graph is a result of careful compensation for nonlinearities in all stages of mask manufacture, including film response and photoresist response.

Near-Field Defects

Near-field defects are small-scale regions of high slope in the surface of the distributed phase plate. They are caused by either defects in the photoresist spinning process or imperfections in the mask used to expose the photoresist. Near-field defects produce regions of high intensity fairly close to the DPP surface, which could damage other optics in the vicinity.

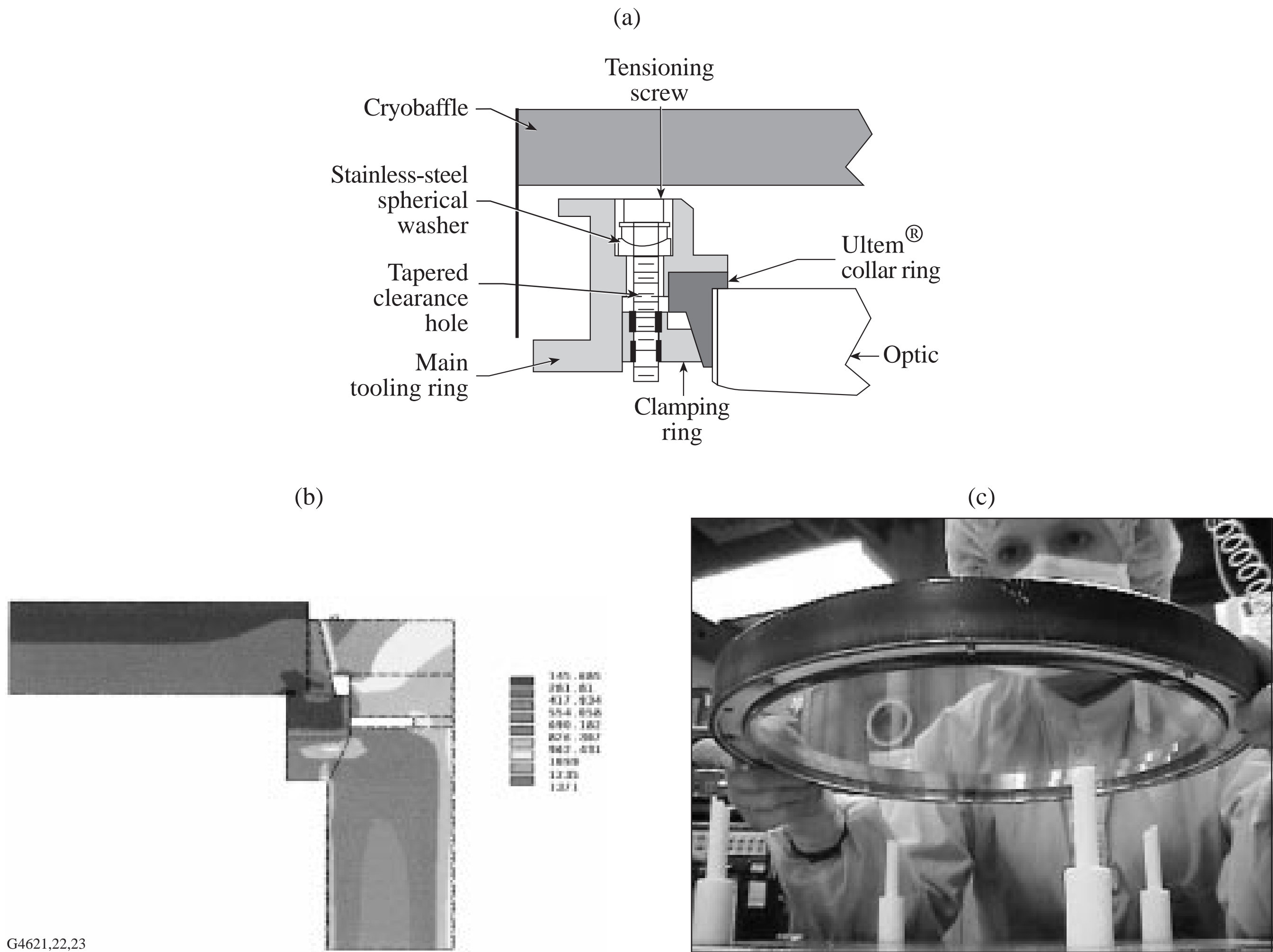

Figure 74.18
(a) The vacuum chuck holds the optic in compression with a Ultem® polyetherimide collar. The substrate mount acts as a barrier for ions traveling to the back surface; it also allows rear radiative cooling and optical monitoring through the optic. (b) Finite element analysis of the substrate in a fully tightened and cooled (–80°C) chuck determined that stresses in the optic would be well below the tensile strength of fused silica. The chuck is tightened enough to prevent the optics from falling out at the high-temperature extreme (+80°C). (c) A close-up view of the chuck on a mounting jig shows the optic, the Ultem® ring, and the tensioning screws. The mount is painted black to increase the infrared emissivity of the aluminum.

In OMEGA, near-field defects could damage the aspheric focusing lens, which is approximately 150 mm in front of the DPP. This lens is both expensive and difficult to replace.

During the production of the first set of replicated DPP's made in epoxy, the near-field defects were removed by locally altering the topography around the defect. Several methods for achieving this were attempted and tested by placing a repaired DPP and a surrogate focus lens in a full beam of OMEGA. The technique that prevailed in both the epoxy and the photoresist materials was to use a hot, blunt point to change the topography of the epoxy by melting. In these cases, the light striking the repaired area is scattered into a wide angular area. The repaired defect areas appear as small holes in the propagating beam.

For etched DPP's, near-field defects were repaired by altering either the photoresist master prior to etching or the fused-silica surface after etching. In silica the near-field defects were repaired by localized grinding with a small dental grinder. Since the etch ratio of silica to the photoresist is 1.3:1, a defect that causes a small modulation in photoresist will turn into a defect with a larger modulation in silica. For this reason, when making etched DPP's, it was preferable to inspect and repair the final etched surface.

DPP's were first inspected for near-field defects in a collimated beam at $\lambda = 442$ nm, which is fairly close in wavelength to the 351-nm wavelength of the OMEGA laser but still visible to the unaided eye. A shadow image of the collimated beam was examined against a white background at a distance of ~150 mm beyond the part. After mapping out the near field for regions of high intensity, a quantitative measure of intensity from each defect was obtained with a CCD camera in the near-field plane (see Fig. 74.21). If the near-field defect caused a peak intensity that exceeded the background by a factor of 3, the defect was marked and removed by grinding [see Fig. 74.21(c)]. During production, plates typically exhibited five to ten defects. Plates with as many as 20 defects were repaired and used on OMEGA. Near-field defect repair was one of the most time-consuming and labor-intensive operations in the manufacturing of DPP's. After being repaired, the optic was cleaned and sol-gel coated by dip coating.

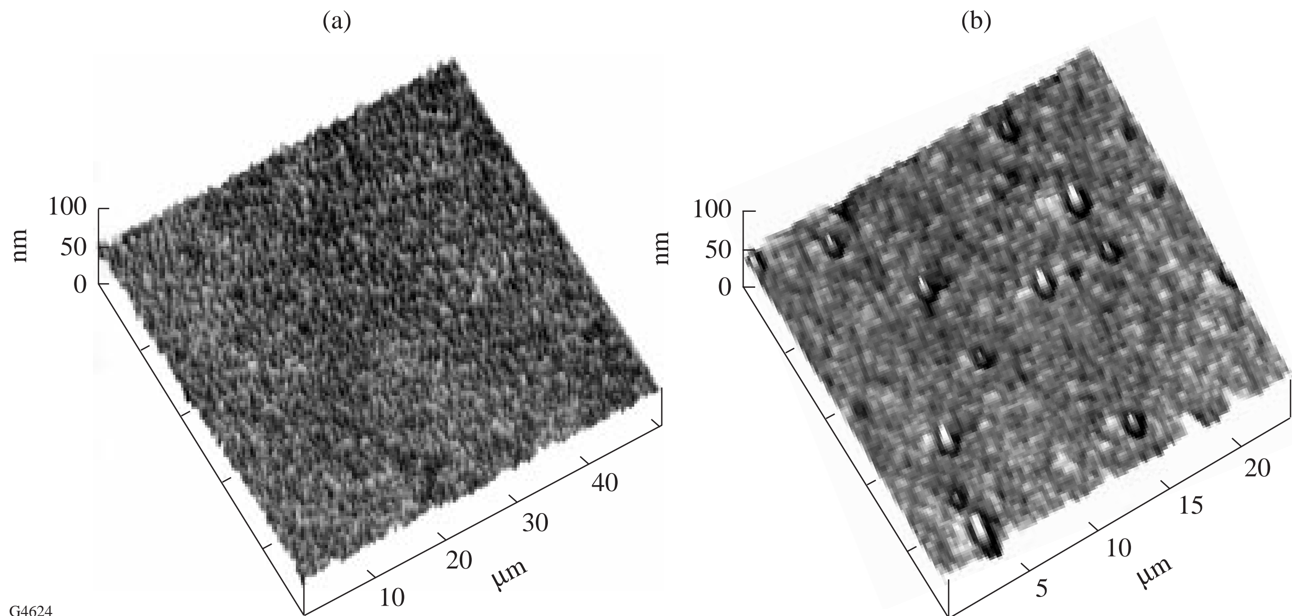

Figure 74.19
(a) The improved surfaces of a DPP cooled during etching can be seen in this AFM scan of a low-scatter area. The rms roughness = 3.4 nm; the P–V roughness = 24.5 nm. (b) AFM scan of worst-case scatter on a production DPP. Scatter was associated with a region that would not have been effectively cooled by the cryobaffle, such as the optical monitor port. The rms roughness = 4.1 nm; the P–V roughness = 60.8 nm. Isolated defects cause most of the scatter losses from this surface. Note the different scale lengths in the two AFM images.

Production Process/Results

A schematic of the full ion-etch system is shown in Fig. 74.22(a). The geometry of the ion source and the substrate can be seen in the photograph of the vacuum chamber's interior [Fig 74.22(b)]. A control program that would shut off the source after a set interval monitored the ion source. The program would terminate the etch if the ion source operated outside the prescribed parameter space for the ion-beam neutralizer emission current and the accelerator (grid) current. The chamber was loaded during the day and operated at night. A typical 14-h etch run included time to heat up the cryobaffle and the substrate to room temperature before removing the part for testing the next morning.

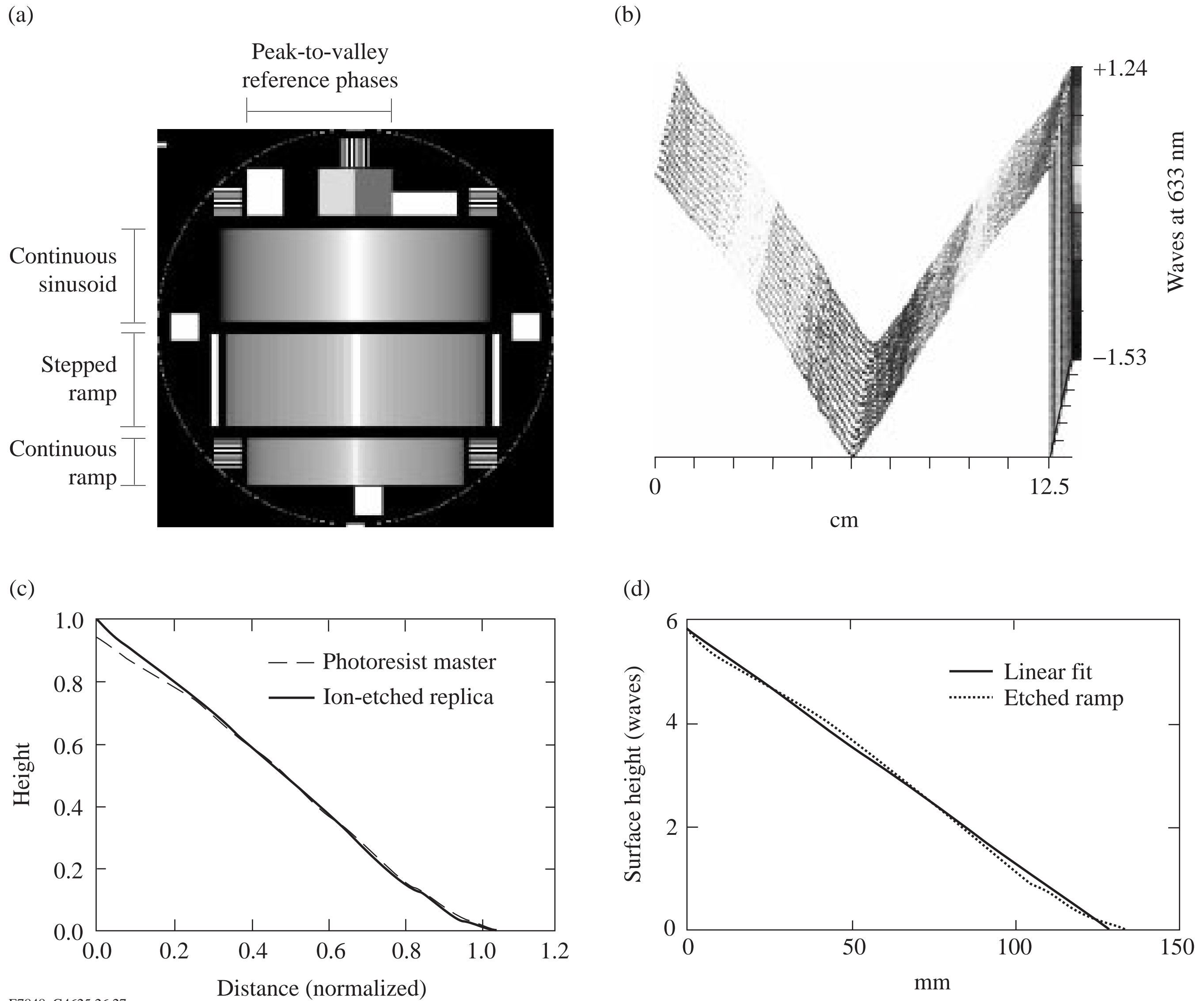

Figure 74.20
(a) The calibration mask is used to characterize both lithographic and etch nonlinearities. (b) A typical interferometric measurement of a continuous calibration ramp. (c) The measured continuous ramps for both silica and photoresist are closely matched and therefore indicative of a highly linear process. The heights are normalized for easy comparison. (d) The etched ramp is compared to a desired linear ramp. The final result includes errors of the entire DPP process, including the film errors from several stages of mask writing and enlarging, photoresist errors, and final etching.

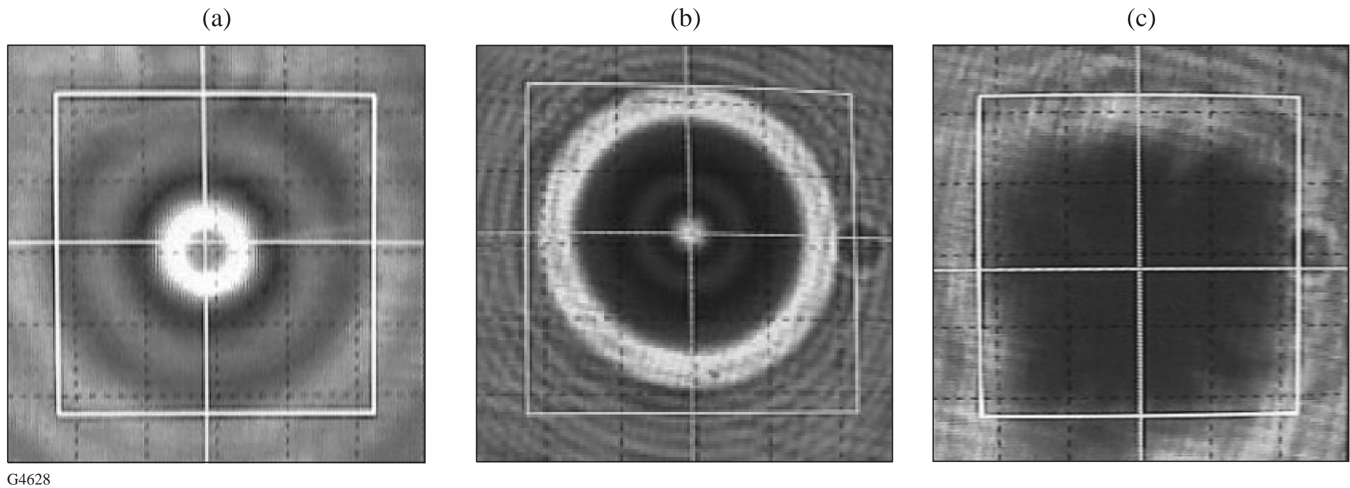

Figure 74.21
A CCD camera is used to analyze individual defects. Several type of near-field defects are found in the DPP's, including lenslets (a), comets (b), goobers, worms, and dirt (last three not illustrated). The final frame (c) shows the near-field result after repair.

An optical monitor measured the thickness of photoresist during an etching run to determine the etch rate and assist in endpoint determination. The DPP design was modified to produce the thickest area of photoresist in the center of the substrate, which was made to coincide with the center of the substrate rotation. A white-light beam was co-aligned with this point to allow for continuous monitoring by interference through the photoresist. The beam entered a monochromator/detector combination, and the signal was fed into a strip chart recorder. The etch rate derived from this measurement proved to be a good indicator of ion-source performance. Ion etching would continue for 30 min after the interference signal ceased to ensure that all the photoresist was removed.

The full production process for DPP's is summarized in the flowchart in Fig. 74.23. The process requires that a photoresist master be made for each etched phase plate. The DPP's for OMEGA were produced over a period of 19 weeks. During this time 79 successful etch runs—66 DPP's and 13 calibration or uniformity checks—were completed. Maintenance occurred on 9 days, and 5 etch runs resulted in failures. A high level of preventive maintenance was performed on the vacuum pumping system and the mechanical components just prior to the final calibration sequence.

Laser-induced-damage thresholds of ion-etched silica always increased when care was taken to prevent the occurrence of redeposition from sputtered tooling. Ion-etched samples of Corning 7940 fused silica were damage tested at 1ω and 3ω with 1-ns pulses. The results are compared to polished and cleaved surfaces in Fig. 74.24. The damage thresholds of the ion-etched surfaces increased over polished surfaces but were less than those for a freshly cleaved surface. The current explanation for the increase is that polishing processes produce both a hydrated layer and a layer of subsurface fractures that can trap absorbing contaminants during the polishing process. The ion-etch process removes the hydrated layer and the layer of fractures and associated contaminants, while the relatively low-energy ions do not penetrate and disrupt the structure near the surface.

A DPP's optical performance can be evaluated by examining the minimum spot size it produces when used in a focusing system similar in aperture and focal length to that found on OMEGA (265-mm aperture, 1800-mm focal length). The spot size is measured at the width corresponding to 5% of the maximum energy. A Gaussian function is fit to the measurement, and the order n (shape) of the function is found. The results for both the replicated epoxy and ion-etched DPP's are given in Table 74.I, and histograms for both DPP types are given in Fig. 74.25. The etched DPP's had a more consistent spot size than the replicated DPP's. Note that the target size had changed between the time the two sets were made. The Gaussian order for the ion-etched set was lower that the target value of 3, but most of those variations were probably due to errors in the mastering process and are not inherent to etching.

(a)

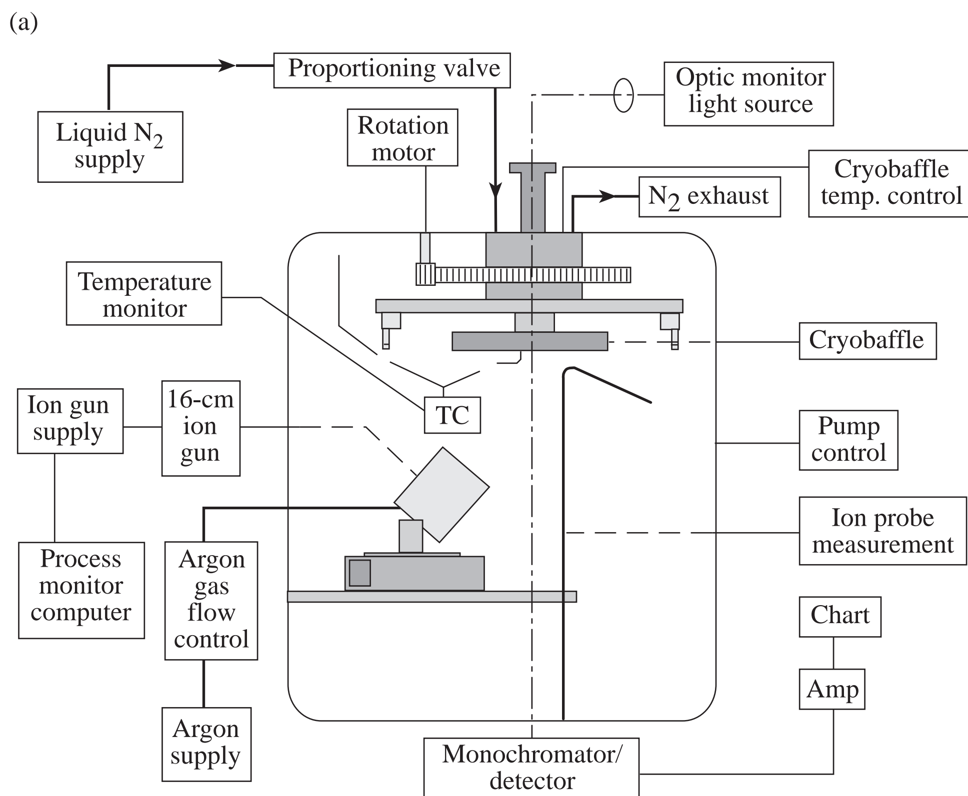

(b)

Figure 74.22
(a) Schematic of the LLE/OMAN 16-cm-ion-source etching system. The system was operated continuously for 14 h during each etch. (b) The 16-cm ion source (below) is shown on a rail in the 54-in. chamber with a substrate in the rotation fixture (above).

A

Start → Incoming inspection → Inspection and clean for AR coating — Pass → Dielectric AR @ 360 nm (one side only) → Cleaning for OISG → Coat master within

Fail → Attach failed optic traveler → Rework surface

Pass attach travelers and maps

PR inspection — Pass → Expose through mask → Develop bleach and bake → Test for spot size → Bake PR coated masters → RASCAL measure center thickness

Fail → Strip PR → A

Fail → Strip PR → A

(map NF repair PR) → Ion etch 54" → Visual inspect → OISG for field test — Pass → NF inspect silica — Pass → Strip dielectric and AR coating

Fail → Rework

Fail → Grind NF defect in SiO_2

B

Cleaned & inspected — Pass → Sol-gel coat @ 351 nm → Spectral test — Pass → R% test — Pass → FF efficiency test — Pass → Mount

Fail → B

Fail → B

Fail → Rework

On system → Stop

OISG: Optical Imaging and Science Group

G4631

Figure 74.23
Flowchart of etched DPP production steps. The substrates were coated initially with a durable antireflection coating to reduce interference effects during exposure of the photoresist.

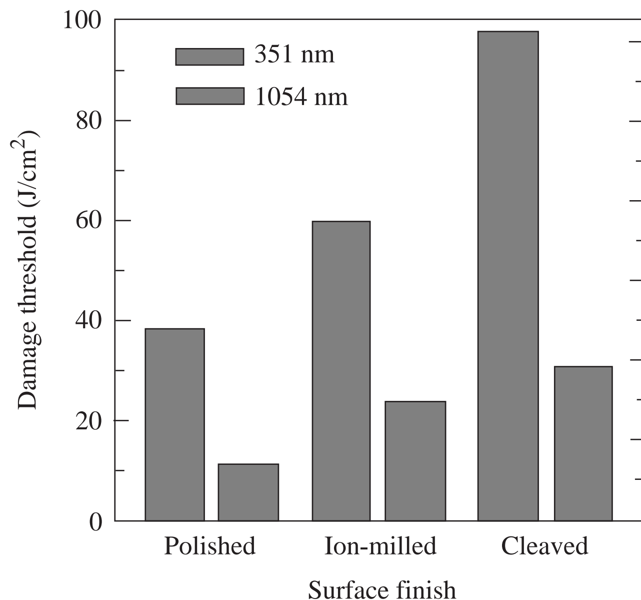

Figure 74.24
Ion etching improves the damage threshold at both 1ω and 3ω for 1-ns pulses.

The transmission through a DPP was measured by collecting all of the energy in the spot using an oversized detector and then reducing the aperture of the detector to 1 mm. The first measure indicates the performance of the sol-gel coatings and scatter characteristics of the piece. The second measure gives the energy likely to impinge on a target and is more relevant to performance on OMEGA. The distribution of the 1-mm aperture measurements for the 60 DPP's used on OMEGA is seen in Fig. 74.26. The plates are near the theoretical maximum transmission for the Gaussian order of $n = 2.44$.

Conclusion

Inert ion etching is a powerful tool for use in manufacturing DPP's for high-peak-power lasers. In concert with gray-level photoresist methods developed at LLE, it provides a method of transferring any continuous function onto an optical surface. The development and production time of 15 months was relatively short given the excellent performance of the devices.

The inert-ion-etching process may be invaluable as a tool for increasing the damage threshold of silica surfaces in both

Table 74.I. Comparison of performance results for 60 etched DPP's manufactured for OMEGA and earlier replicated epoxy DPP's.

	Etched DPP's		Epoxy DPP's	
	Mean	1 σ	Mean	1 σ
Minimum spot size, μm	936.7	14.1	635.8	37.6
Gaussian order	2.44	0.07	~	~
Full transmission	0.994	0.004	Degraded	~
T @ 1-mm aperture	0.959	0.006	~	~

~ no data available.

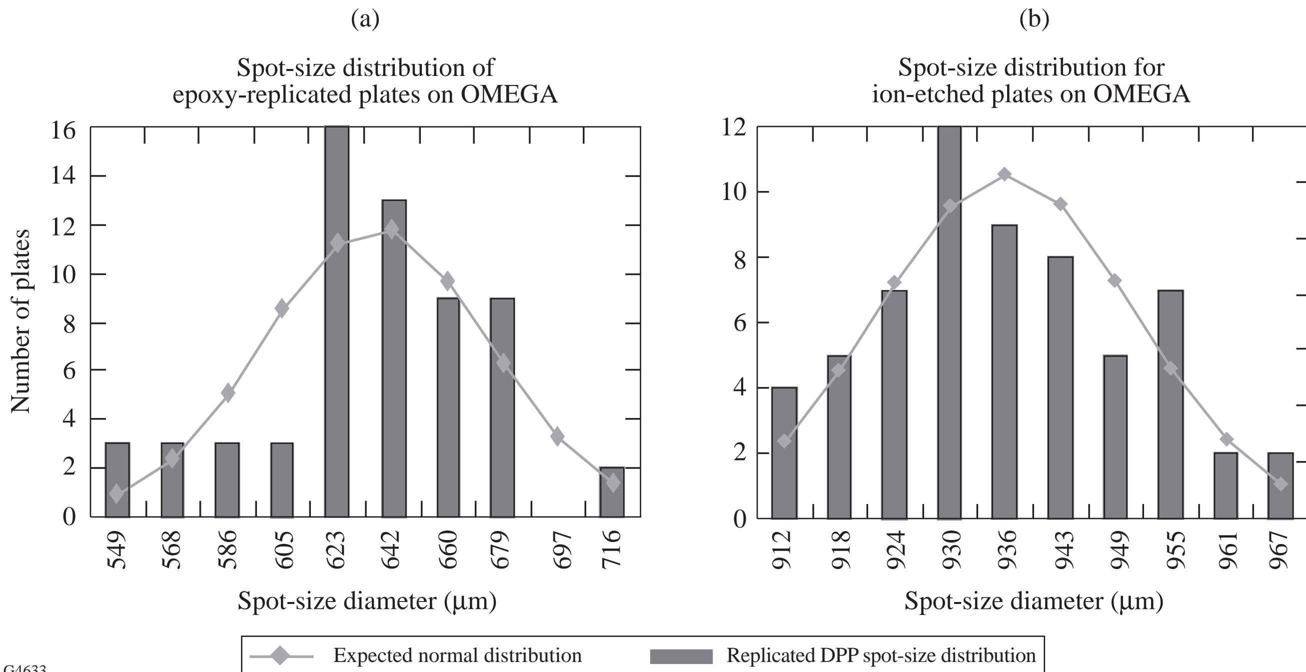

Figure 74.25
The far-field spot size (at the 5% of maximum width) was measured for each DPP. The distribution of spot sizes for the epoxy-replicated DPP's (a) was much broader than in the ion-etched DPP's (b).

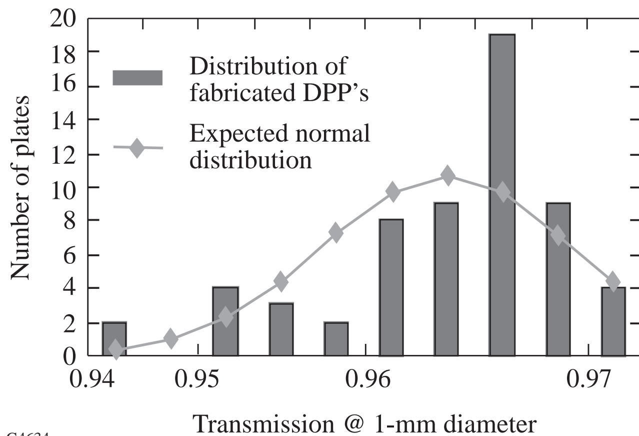

Figure 74.26
Despite some loss due to the near-field defect repairs and slight scatter, the transmission was near the maximum value possible for this Gaussian order. The DPP design requires that some of the energy be sent outside the target.

the infrared and the UV. Ion etching will be tested on other components of OMEGA to assess its capabilities for raising laser-damage thresholds.

ACKNOWLEDGMENT

This work was supported by the U.S. Department of Energy Office of Inertial Confinement Fusion under Cooperative Agreement No. DE-FC03-92SF19460, the University of Rochester, and the New York State Energy Research and Development Authority. The support of DOE does not constitute an endorsement by DOE of the views expressed in this article.

REFERENCES

1. Laboratory for Laser Energetics LLE Review **65**, 1, NTIS document No. DOE/SF/19460-117 (1995). Copies may be obtained from the National Technical Information Service, Springfield, VA 22161.
2. Laboratory for Laser Energetics LLE Review **71**, 101, NTIS document No. DOE/SF/19460-186 (1997). Copies may be obtained from the National Technical Information Service, Springfield, VA 22161.
3. Laboratory for Laser Energetics LLE Review **64**, 170, NTIS document No. DOE/SF/19460-99 (1995). Copies may be obtained from the National Technical Information Service, Springfield, VA 22161.
4. Y. Lin, T. J. Kessler, and G. N. Lawrence, Opt. Lett. **20**, 764 (1995).
5. G. K. Wehner and G. S. Anderson, in *Handbook of Thin Film Technology*, edited by L. I. Maissel and R. Glang (McGraw-Hill, New York, 1983), p. 3-17; G. C. Schwartz, in *Handbook of Semiconductor Interconnection Technology*, edited by G. C. Schwartz, K. V. Srikrishnan, and A. Bross (Marcel Dekker, New York, 1998), pp. 1–76.
6. O. Auciello and R. Kelly, eds., *Ion Bombardment Modification of Surfaces: Fundamentals and Applications*, Beam Modification of Materials, Vol. 1 (Elsevier, Amsterdam, 1984).
7. B. A. Banks, in *Handbook of Ion Beam Processing Technology: Principles, Deposition, Film Modification, and Synthesis*, edited by J. J. Cuomo, S. M. Rossnagel, and H. R. Kaufman (Noyes Publications, Park Ridge, NJ, 1989), pp. 338–361.
8. E. Chason and T. M. Mayer, Appl. Phys. Lett. **62**, 363 (1993).
9. T. Motohiro and Y. Taga, Thin Solid Films **147**, 153 (1987).
10. S. R. Wilson *et al*., in *Science of Optical Finishing*, Vol. 9, 1990 Technical Digest Series (Optical Society of America, Washington, DC, 1990), p. 73.
11. H. R. Kaufman, R. S. Robinson, and W. E. Hughes, *Characteristics, Capabilities, and Applications of Broad-Beam Sources* (Commonwealth Scientific Corporation, Alexandria, VA, 1987).
12. J. M. E. Harper, J. J. Cuomo, and H. R. Kaufman, J. Vac. Sci. Technol. **21**, 737 (1982).
13. H. R. Kaufman, *Fundamentals of Ion-Source Operation* (Commonwealth Scientific Corporation, Alexandria, VA, 1984).
14. Commonwealth Scientific Corporation, Alexandria, VA 22314-1974.
15. O. Auciello, in *Ion Bombardment Modification of Surfaces: Fundamentals and Applications*, edited by O. Auciello and R. Kelly, Beam Modification of Materials, Vol. 1 (Elsevier, Amsterdam, 1984), Chap. 1; G. Carter and M. J. Nobes, *ibid*., Chap. 5.
16. M. Jin, "Numerical Estimation for 8-cm Ion Source Distribution," Internal Memo, Laboratory for Laser Energetics, University of Rochester (8 August 1991).
17. Atomic force microscope contact mode, Model NS3, Digital Instruments, Inc., Santa Barbara, CA 93117.
18. Vacuum Process Technology, Pembroke, MA 02359.
19. Ultem®-Polyetherimide, available from Design Engineering Plastic Products, Reading, PA 19612-4233.
20. Fused silica available from Technical Products Division, Advanced Products Department, Corning Glass Works, MP-21-4, Corning, NY 14831.
21. Zygo Mark IVxp, Zygo Corporation, Middlefield, CT 06455.